Numerical Analysis of the Von Karman Nose Cone and Volume Reduction Though Topology Optimisation

ARDRIT RAMADANI

Abstract

The structural integrity of a Brass Von Karman nose cone model is analysed to determine its suitability for supersonic flow testing. It was found to be capable of handling the total and shear pressure profile found through a CFD analysis of the flow field, with a safety factor of 1.35 to yield. The nose cone was subject to topology optimisation, finding the minimum volume in which it would not buckle or fail to be 20% of the original internal volume.

Contents

1. Introduction (Part 1)

1.1. The model

This paper sets out to investigate the structural integrity of a scale model of a Von Karman rocket nose cone, of ratio 5:1, for use in a supersonic wind tunnel with a free flow Mach number of 2.0. The model is being manufactured to validate computational flow models of the nose cone, as well as for future teaching applications, and a structural analysis is required to ensure that the experimental model does not fail in the wind tunnel causing damage to the testing equipment or injury to technical staff. The model is to be capable of multiple uses and the maximum stress must therefore not exceed the yield strength of the material as to not cause permanent deformation of the aerodynamic profile.

1.2. Definition and properties

The proposed model is to be built out of Free-Cutting Brass, UNS C36000, for its suitability for high-speed machining making it manufacturable within the available workshop while also having a relatively low cost and being readily available.

Table 1: Material properties of UNS C36000 brass. (ezlock.com)

	Modulus of elasticity (MPa)	Poisson Ratio	Yield Strength (MPa)	Ultimate Tensile Strength (MPa)	Density (tonne/mm^3)
UNS C36000	97E+3	0.31	310	469	8.4977307E-9

The equations of the Von Karman curve are given parametrically as:

$$\theta(x) = \arccos\left(1 - \frac{2x}{L}\right) \tag{1}$$

$$y(\theta) = \frac{R}{\sqrt{\pi}}\sqrt{\theta - \frac{\sin(2\theta)}{2}} \tag{2}$$

With the characteristic lengths of L = 5inches, R = 0.5inches, and the coordinates flipped to the Y-axis and offset by 127mm in the positive Y-direction.

The nose cone for analysis comprises of a 2mm hole drilled through the centre of the nose cone from the base in order to allow for the extraction of a pressure taping close to the leading edge of the nose cone, the hole to be drilled on the wetted surface is 0.2mm and assumed to be negligible in the scope of the analysis, exclusion of this taping allows the model to be simplified into a 2D-axisymmetric model to reduce computational costs. The wind tunnel mounting and measuring equipment are in the imperial form and measurements are made in inches, the cross-sectional sketch converts to the basis of a mm, N, Tonnes, MPa, SI standard. CFD calculations are caried out to determine the pressure profile and shear forces along the wetted surface of the nose which are to be captured in the FEA modelling. Figure 2 shows the pressure distribution around the nose cone, as the flow is supersonic, the low-pressure region behind the nose cone can be ignored as it does not affect the upstream flow characteristics and the region will be covered by the mounting system of the wind tunnel. The base mount of the nose cone will be milled and the centre hole will be drilled, both processes of which incorporate a slightly rounded tool meaning that a small fillet was applied to the re-entrant corners in order to better match the real surface as well as to reduce the formation of singularities at the theoretically sharp corners which occur in FEA.

1.3. Loads and Boundary conditions

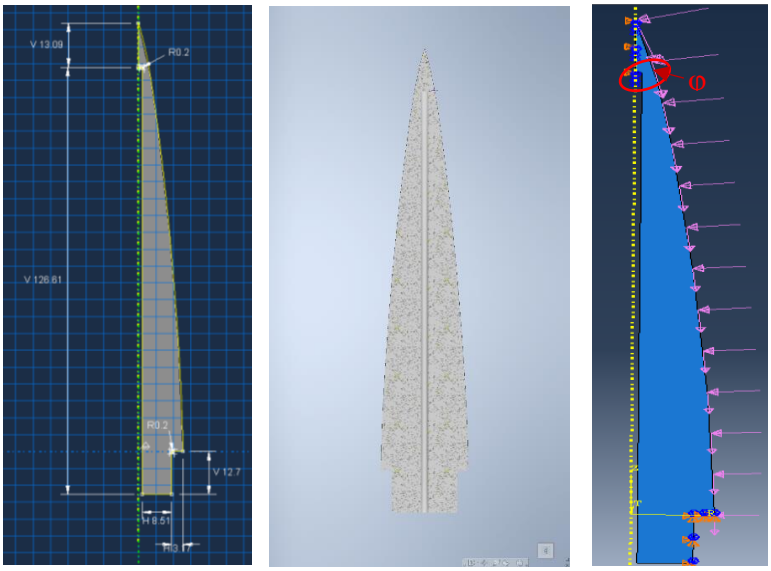

Figure 1: 2D-Axisymmetric (left), 3D-cross section (Middle), Loads and Boundary conditions (Right)

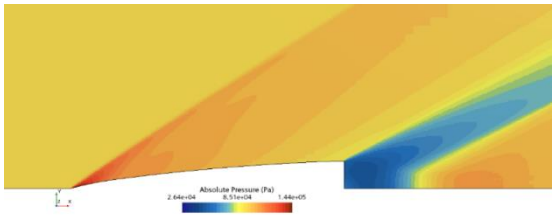

Figure 2: CFD obtained pressure distribution around the axisymmetric nose cone at a free stream Mach number = 2

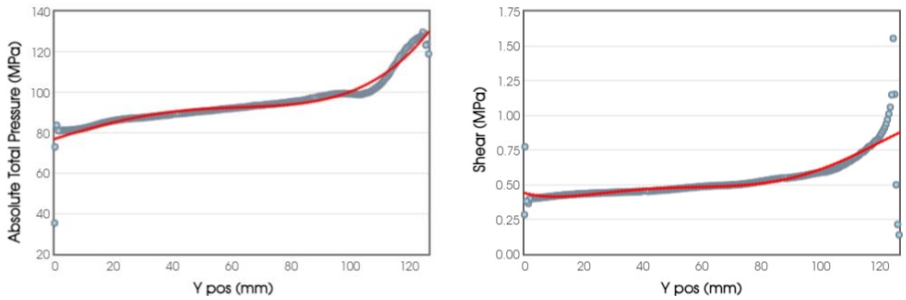

Figure 3: Absolute Total Pressure vs Y position (left) and Shear vs Y position (right) along the nosecone surface

From Figure 3, a fourth order polynomial approximation can be applied, shown as the red line, to determine the spatially dependent Shear and Absolute pressures on the wetted surface. The approximated equations are:

$$Total\ Pressure = 0.00009Y^3 - 0.01483Y^2 + 0.84737Y + 74.53587 \quad (3)$$

$$Shear = 0.0000000052Y^4 - 0.0000007266Y^3 + 0.0000353884Y^2 + 0.000465213Y + 0.4153444147 \quad (4)$$

The loads are applied as a Pressure, and a Shear Surface Traction pressure acting on the wetted curved surface of the nose cone, into the body and towards the negative Y axis with a unit magnitude as the Total and Shear pressure distribution equations appropriately scale the pressures along the surface. Analytical Fields are created to represent this distribution with equations (3) and (4) respectively. The mounting hardware fixes the nose cone in the centre of the wind tunnel and allows for zero degrees of freedom at the base of the nose cone, thus the boundary conditions at the base of the nose cone constrain all movement and rotation to zero. An X-Z plane displacement and rotation constraint is also set near the leading edge of the nose

cone where the volume meets the symmetry axis. The symmetry axis is defined as the vertical Y-axis, around which an axisymmetric revolution of the cross section will be taken.

1.4. Meshing and assumptions

Due to the unique shape of the nozzle and the large portion being a curve, while a structured mesh could prove more efficient, the generation of a structured mesh will inevitably be cause for errors and failure in the meshing process. A free mesh will therefore be utilised as the additional computational cost is outweighed by the increased accuracy and suitability for the shape being investigated, various element types will be used to ensure that solutions are not mesh dependent including triangular, quad, quad dominated, linear and quadratic elements. In order to reduce errors in convergence, the filleted corners will be seeded to have at least 4 points on the curve which will reduce the formation of singularities.

The maximum stress is assumed to be at the end of the drilled hole close to the leading edge, shown on Figure 1 (Right) labelled as region φ, due to the reduced wall thickness at this point and the gradient of the force distribution being highest at the leading edge. Analysis of the maximum stress in this region will be used as a variable in the determination of a converged and mesh independent result.

2. Mesh Convergence

2.1. Quad

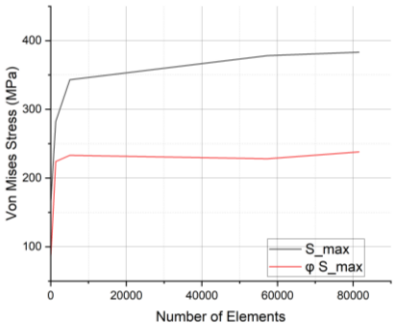

Figure 4: Quad - Linear

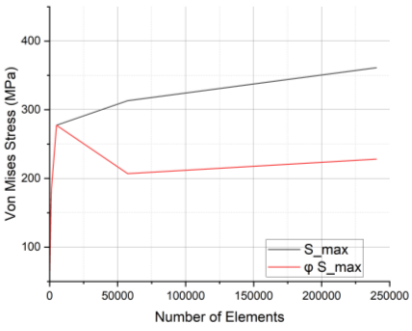

Figure 5: Quad Quadratic

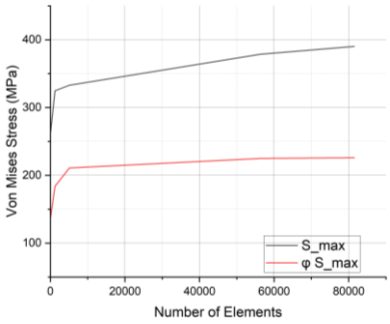

Figure 6: Quad Dominated

2.2. Triangle

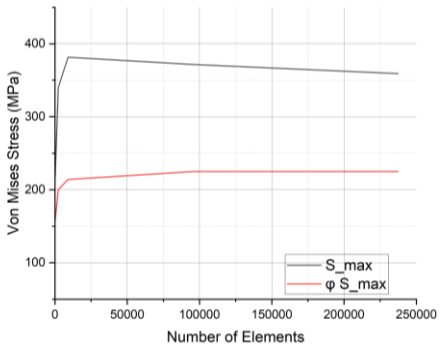

Figure 7: Triangle - Quadratic

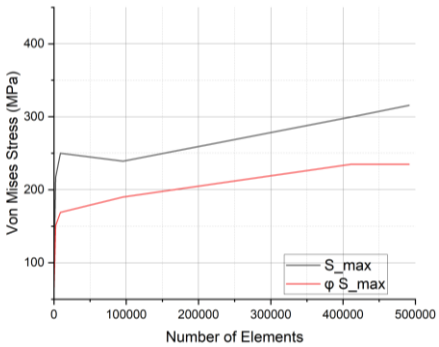

Figure 8: Triangle - Linear

3. Results

Table 2:Converged results for each mesh type

		Element size for convergence (mm)	Number of Elements for convergence	S_{max} (MPa)	S_{max} at φ (MPa)
Triangular	Linear	0.075	410793	299.7	235
	Quadratic	0.15	95633	371.7	225
Quad Dominated		0.15	56336	378.7	225
Quad	Linear	0.075	240180	361.1	228
	Quadratic	0.5	5075	343	233

Table 3: Mesh independent result and safety factors

	Max stress (MPa)	Yield Strength (MPa)	Ultimate Tensile Strength (MPa)	Safety factor to Yield	Safety factor to failure
Nose Cone (UNS C36000)	229.2 ± 5	310	469	1.35	2.05

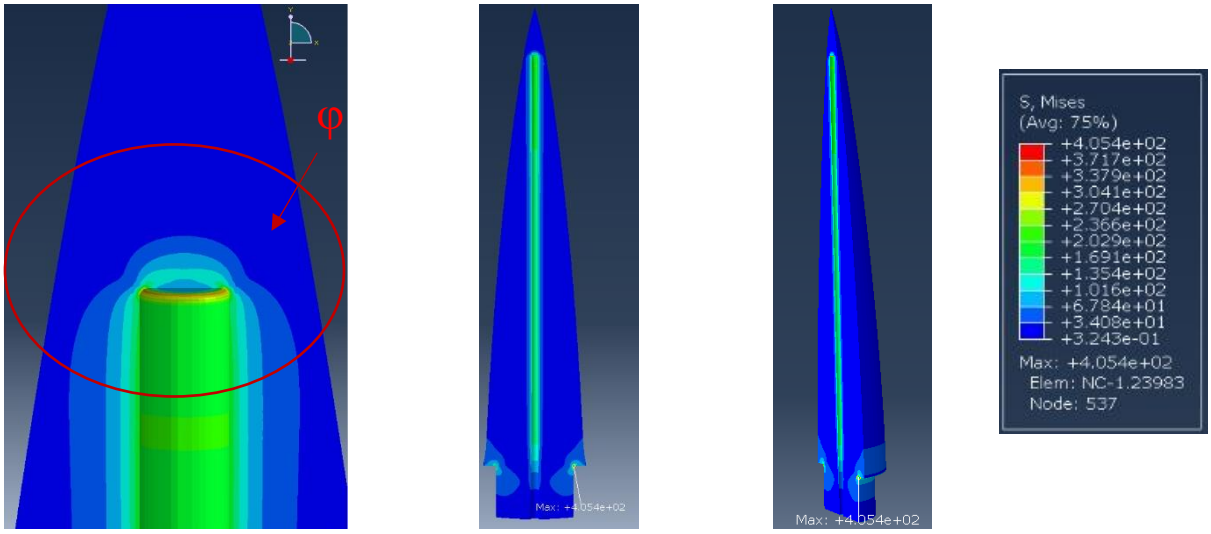

Figure 9: Von Mises stress distribution, Region of interest (Left), Frontal cross section (Middle), Wetted surface (Right)

4. Discussion

The geometry analysed is one that poses several problems for the application of a numerical FEA, having both a unique shape and several re-entrant corners. As expected the re-entrant corner on the mounting boundary produced a singularity even with the slight fillet which was implemented, this can be seen mostly in the Linear solvers where the maximum Von Mises value was on the fillet and failed to converge to a finite value within the licenced capability. The Quadratic solvers for both the quadrilateral and triangular element types managed to mostly resolve the singularity into a stress concentration however the value achieved is higher than what is expected and found from previous models. The stress concentration at the base would suggest a permanent deformation or failure at that point as the stress is above the yield strength of the material, however, as previous models used the same material and mounting system and did not suffer such failures, it can be assumed that the stress concentration at this point of maximum stress is incorrect. Furthermore, St. Venants principle states that for a singularity perturbation, the error is a local phenomenon and can be assumed to not affect the validity of the global model (Givoli, D. 1993). Taking the stress from an adjacent node on the

fillet supports this hypothesis as the results were in line with theory and close to the maximum ~230 MPa stress found at the area of interest φ.

Taking the maximum Von Mises stress in the region of interest φ, near the leading edge of the nose cone, as the variable for a mesh sensitivity study it can be seen that the solution is entirely independent of the type of element or order of solver with an unstructured mesh. A structured mesh was attempted to be used but critical errors would cause failure of the meshing process for meshes finer than 2mm, courser than which convergence could not be achieved, supporting the assumption that a structured mesh would be unsuitable for this application. The stress can be seen to converge to a value approximately 229±5 MPa regardless of the mesh used and there is high confidence in the global validity of the results obtained, applying St. Venants principle and ignoring the singularity with is infinitely far from the area of interest on the local scale. The second polynomial order basis functions showed for both element types to produce converged results with a larger element size and significantly less elements, this is due to the extra interpolation points providing more nodes per element with the higher polynomial order basis functions, essentially increasing the resolution of a single element, with a linear triangle having 3 nodes and a quadratic triangle having 6, and a quadrilateral linear element having 4 nodes and a quadratic element having 9. The larger increase in nodes between polynomial orders in quad elements over triangle elements also supports the larger difference between converging sizes of quadratic vs linear elements of each type, with a quadratic triangle achieving convergence with an element size twice that required by a linear triangle, and a quadratic quad being able to achieve convergence with an element size 3 times greater than that of a quadratic triangle and 6.7 times greater than that of a linear quad or triangle.

The study has shown that the model in question produces a safety factor of 1.35 to yield, meaning that, under the scope of its intended use, no permanent deformation would be caused and the model could be used repeatedly due to brasses additional strong ability to withstand cyclic loading. This would suggest that the central hole could potentially be drilled deeper in future models to produce a pressure taping closer to the leading edge for more relevant pressure readings. Additionally, the safety factor to failure is 2.05 which is excessive for use cases where the part is disposable, such as that of a launch of a real rocket, meaning that the internal volume could be reduced to reduce the total weight of the rocket while still providing adequate rigidity and stress tolerance.

The pressure and shear distribution along the wetted surface was represented as a spatially dependent variable in order to reduce singularities from other methods, such as a distribution of point loads, and is believed to the most accurate representation. It must be noted from Figure 3 that while the pressure distribution is accurately captured, the shear distribution is not entirely accurate at the leading edge and could slightly misrepresent the pressure very close to the tip however as that section is solid and the total shear force is small, this should not present doubt in the validity of the analysis. In future a higher polynomial approximation or an additional point load towards the leading edge could be incorporated to better encapsulate the shear distribution.

5. Optimisation (ATOM) (Part 2)

5.1. Problem setup

The Von Karman nose cone analysed in (Part 1) is to be incorporated into a rocket for use in a single launch, the material properties and shape are as previously described in 1.2 and 1.3. The optimisation aims to reduce the internal volume while maintaining the shape of the wetted surface and boundaries to ensure the aerodynamic performance and mounting hardware are not affected by the optimisation. The investigation will analyse the effects of mesh resolution on the results of a computational topology optimisation and employ its use in the reduction of the volume to a targeted 10,20,30 and 40% of the original volume.

5.2. Design Response, Objectives, and Constraints

The target objective of the optimization is to reduce the strain energy of the nose cone in order to maximise stiffness. The optimization will incorporate several design responses including Strain Energy, Volume, and Stress. The optimization must maintain the minimum centre hole diameter of 2mm, external surface area and shape, and mounting surface. The yield strength may be exceeded as it is a single use part, however the total stress must not exceed the Ultimate Tensile Strength (UTS) of the material in order to not fail or buckle during use.

Table 4: Design response and constraints

Design Response	Type	Value
Strain Energy	Objective	Minimum
Volume	Constraint	<= 10,20,30,40 (%)
Stress	Constraint	<= 410 (MPa) UTS

5.3. Effects of mesh

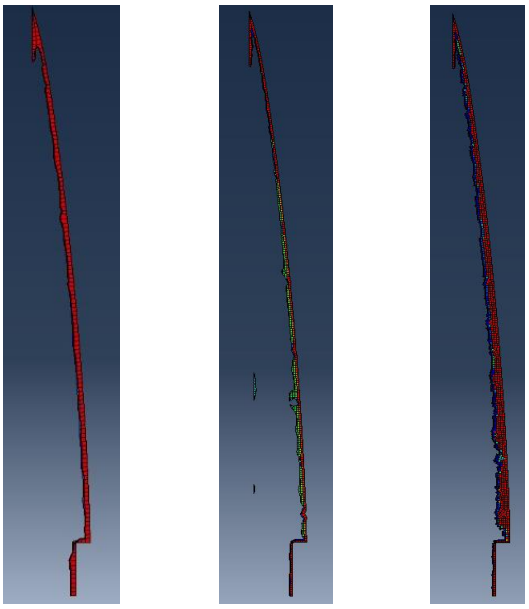

Figure 10: Optimization for Mesh size = 1mm (left), 0.5mm (middle), 0.126mm (Right)

The mesh resolution is an important factor to consider when setting up an optimization task as it defines the resolution at which volume subtractions can be made. With a finer mesh allowing for the removal of smaller increments of volume (Bendsøe, M.P. 2003), and for instances where a large portion of the model is constricted, such as the large surface are of the nose cone, a large mesh size can fail to remove any volume as the smallest increment size can be larger than the maximum allowable free volume reduction. Figure 10 shows the resolution for mesh sizes of 1,0.5, and 0.126mm.

5.4. Results

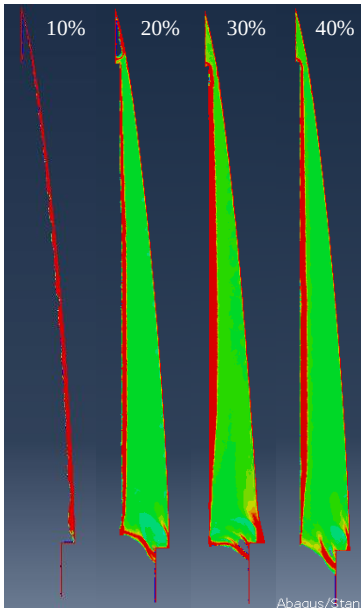

Figure 11: Optimization results at X% of original volume

5.5. Discussion

From 5.3 it was found that a mesh size of 0.25mm produced an adequate solution while also minimizing computational costs. Figure 11 shows the results from volume constraints of 10,20,30 and 40%, where it can be seen that the main location for the removal of volume is within the base, the centre hole diameter can be slightly increased, and the leading edge section can be hollowed out. The study also showed that a maximum reduction to 20% was possible as the 10% volume could not maintain a maximum stress below the UTS.

While the reduced volume regions would produce a substantial decrease in weight, not all of the reductions are practical in an industrial scenario. The centre hole can be drilled with a wider drill bit and the base could be further hollowed out, however, the hollow region near the leading edge would not be possible to be removed by current industrial manufacturing techniques.

6. Conclusion

The structural analysis of the Von Karman nose cone showed that the proposed design had a safety factor of at least 1.35 and could be approved for use within the high speed wind tunnel. The solution is believed to have high confidence as the results achieved were independent of the mesh used, element type or polynomial order of basis functions. A stress singularity and concentration was found to occur on a re-entrant corner far from the region of interest and was deemed to not affect the validity of the result, in line with St Venant's principle of singularities. The large factor of safety suggests that future models may use a hole drilled closer to the leading edge in order to extract pressure tapings from closer to the edge to provide more valuable data, and that there is room for the topology optimisation reduction of the internal volume.

A topology optimisation study showed that a mesh size of 0.25mm produced adequate resolution for the reduction of internal volume, and that while a significant volume fraction can be removed, at minimum leaving only 20% of the original volume, without compromising the structural integrity, current manufacturing methods are incapable of accurately extracting the volume in an industrial setting.

Reference

Givoli, D. and Rivkin, L. (1993). The DtN finite element method for elastic domains with cracks and re-entrant corners. Computers & Structures, 49(4), pp.633–642. doi:https://doi.org/10.1016/0045-7949(93)90068-o

Bendsøe, M.P. and Sigmund, O. (2003). Topology optimization : theory, methods and applications. Berlin: Springer.